The Displaced Rectangular Waveguide Junction and its Use as an Adjustable Reference Reflection

JOHN D. HUNTER, SENIOR MEMBER, IEEE

Abstract—**The reflection from a displaced junction in rectangular waveguide and the equivalent circuit parameters are calculated using modal analysis. The use of weighted Gegenbauer polynomials to describe the field in the plane of displacement is shown to significantly improve the rate of convergence of the solution in comparison to waveguide-type mode functions. Approximate formulas are given for displacements of up to 25 percent of the waveguide dimensions. An *E*-plane displaced junction is suggested for use as an adjustable reference reflection.**

I. Introduction

WHEN TWO collinear waveguides of identical cross section are joined, any misalignment will cause a signal incident on the junction to be partially reflected. In a waveguide system with many junctions, it is possible for the reflections caused by several small misalignments to interfere constructively, and significantly degrade the system performance. The effect of small junction displacements in either the *E*-plane or *H*-plane of rectangular waveguide can be estimated by representing the junction as an iris [1], but this approximation has long been known to produce large relative errors [2].

The displaced junction is amenable to investigation using the modal analysis technique, which has been successfully applied to several other waveguide discontinuity problems [3]–[7]. In most previous applications, the field in the plane of discontinuity has been represented by a series of trigonometric functions appropriate to a waveguide with the same cross section as the aperture. Although these functions each satisfy the boundary conditions in waveguide, several must be summed in order to approximate the field behavior at the aperture edges [6]. It has been suggested that this approximation can be improved by taking into consideration the normally neglected higher order functions [8]. Recently, the use of weighted Chebyshev polynomial aperture functions, which each behave correctly at the edge of a half plane, has been shown to improve the rate of convergence of the matrix solution for a step-diaphragm junction in parallel-plate waveguide [9].

In this paper, the effect of transverse displacement of a rectangular waveguide junction is calculated for TE_{10}-mode propagation. The modal analysis technique is used, with the correct behavior of the transverse electric field near the aperture edges ensured by using appropriately weighted Gegenbauer polynomials as the aperture functions. The rate of convergence of the matrix solutions is compared with that achieved using trigonometric aperture functions. Simple empirical formulas developed from the solutions are more accurate than the usual iris approximations.

An *E*-plane displaced junction is shown to have a simple equivalent circuit, making it suitable for use as an adjustable reference reflection.

Manuscript received June 9, 1983; revised September 27, 1983.

The author is with CSIRO Division of Applied Physics, P.O. Box 218, Lindfield, N.S.W. 2070, Australia.

II. General Formulation

Two rectangular waveguides with identical cross-sectional areas A_1 and A_2 are joined with axes parallel, but with a transverse displacement s normal to either the broad wall (*E*-plane displacement) or the narrow wall (*H*-plane displacement). A TE_{10}-mode field incident on the junction from waveguide 1 has a frequency such that no other propagating modes can be sustained in the guide.

The transverse electric and magnetic fields in the aperture formed in the junction plane can be written as

$$\vec{E}_T'' = \sum_n b_n \vec{e}_n'', \qquad \vec{H}_T'' = \sum_n c_n \vec{h}_n'' \tag{1}$$

with the functions $\vec{e}_n''$ and $\vec{h}_n''$ chosen orthogonal over the aperture area A_a to satisfy

$$\int_{A_a} \vec{e}_i'' \times \vec{h}_j'' \cdot d\vec{A}_a = 0, \qquad i \neq j. \tag{2}$$

The sums of the incident and reflected transverse fields in the incident waveguide are, at the aperture plane

$$\vec{E}_T = \vec{e}_{1,0} + \sum_p a_p \vec{e}_p$$
$$\vec{H}_T = \vec{h}_{1,0} - \sum_p a_p \vec{h}_p \tag{3}$$

where a_p is the complex coefficient of mode p. In waveguide 2, the transverse transmitted fields at the aperture plane are

$$\vec{E}_T' = \sum_p a_p' \vec{e}_p', \qquad \vec{H}_T' = \sum_p a_p' \vec{h}_p'. \tag{4}$$

The mode components $\vec{e}_p$, $\vec{h}_p$ and $\vec{e}_p'$, $\vec{h}_p'$ are orthogonal over A_1 and A_2, respectively.

Equating the transverse fields in the aperture plane enables the vector $\underset{\sim}{b}$ with elements b_n to be determined

0018-9480/84/0400-0387$01.00 ©1984 IEEE

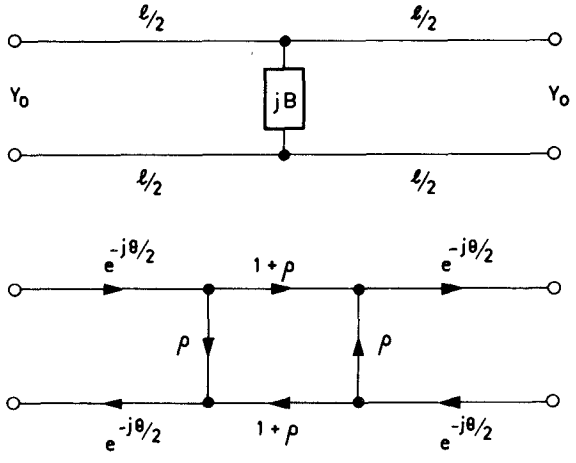

Fig. 1. Equivalent circuit and flow-graph for a displaced waveguide junction.

from the matrix equation [6]

$$\underset{\sim}{A}\underline{b} = \left(\underset{\sim}{S}\underset{\sim}{T} + \underset{\sim}{S}'\underset{\sim}{T}'\right)\underline{b} = 2\underset{\sim}{S}\underline{a}_1 = \underset{\sim}{Q} \tag{5}$$

where $\underline{a}_1$ is a vector with the first element unity and all other elements zero, and the elements of the matrices $\underset{\sim}{S}$ and $\underset{\sim}{T}$ are

$$S_{n,p} = \int_{A_a} \vec{e}_n'' \times \vec{h}_p \cdot d\vec{A}_a \Big/ \int_{A_a} \vec{e}_n'' \times \vec{h}_n'' \cdot d\vec{A}_a$$

$$T_{p,n} = \int_{A_a} \vec{e}_n'' \times \vec{h}_p \cdot d\vec{A}_a \Big/ \int_{A_1} \vec{e}_p \times \vec{h}_p \cdot d\vec{A}_1. \tag{6}$$

The elements of $\underset{\sim}{S}'$ and $\underset{\sim}{T}'$ are given by (6) after replacing $\vec{e}_p$, $\vec{h}_p$, and A_1 by $\vec{e}_p'$, $\vec{h}_p'$, and A_2, respectively. The first coefficient in (3) is the reflection coefficient Γ of the propagating mode in waveguide 1, and is the first element of the vector $\underset{\sim}{T}\underline{b} - \underline{a}_1$.

The junction is symmetric and lossless, and its equivalent circuit may be represented as a shunt susceptance B at the center of a lossless transmission line of real characteristic admittance Y_0 and length l, as shown in Fig. 1 with the corresponding flow-graph. Then

$$\Gamma = \rho e^{-j\theta} = \frac{-j(B/Y_0)\exp(-j\theta)}{2 + jB/Y_0} \tag{7}$$

where $\theta = 2\pi l/\lambda_g$, with λ_g the guide wavelength, and

$$\left|\frac{B}{Y_0}\right| = \frac{2|\Gamma|}{\left[1-|\Gamma|^2\right]^{1/2}}$$

$$\arg(\Gamma) = -\operatorname{sgn}\left(\frac{B}{Y_0}\right)\left[\pi - \cos^{-1}(|\Gamma|)\right] - \theta. \tag{8}$$

The sign of B/Y_0, denoted by $\operatorname{sgn}(B/Y_0)$, is $+1$ when B is capacitive, and -1 when B is inductive.

III. *E*-Plane Displacement

The displaced junction in Fig. 2 shows waveguide 2 in the x, y', z cartesian coordinate system displaced by an amount $y = s$ with respect to waveguide 1 in the x, y, z cartesian coordinate system. With a TE_{10}-mode signal incident from waveguide 1, the TE_{1p} and TM_{1p} modes set up

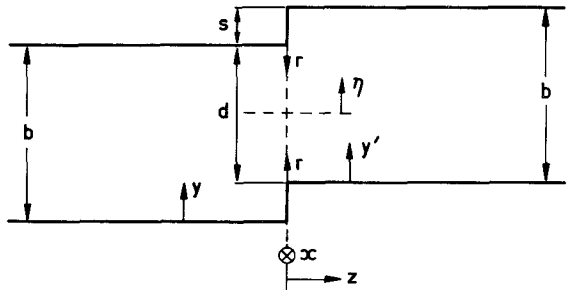

Fig. 2. Geometry of an *E*-plane displaced junction.

by the discontinuity will combine to ensure $\vec{E}_x = 0$, and form the LSE_{1p} mode with components

$$\vec{e}_p = \hat{y}\sin\left(\frac{\pi x}{a}\right)\cos\left(\frac{p\pi y}{b}\right), \qquad p = 0,1,2,\cdots$$

$$\hat{x}\cdot\vec{h}_p = \frac{j\omega\epsilon b}{2\pi\gamma_p}\left[\left(\frac{\lambda}{2a}\right)^2 - 1\right]\sin\left(\frac{\pi x}{a}\right)\cos\left(\frac{p\pi y}{b}\right) \tag{9}$$

where $\vec{e}_{1,0} \equiv \vec{e}_0$. γ_p is related to the propagation constant γ_p' of mode p, which is evanescent for $p \geq 1$, by

$$\gamma_p = \frac{b}{2\pi}\gamma_p' = \left[\left(\frac{p}{2}\right)^2 - \left(\frac{b}{\lambda_g}\right)^2\right]^{1/2}, \qquad p = 1,2,3\cdots$$

$$\gamma_0 = j\beta_0 = j\frac{b}{\lambda_g}. \tag{10}$$

Expressions for $\vec{e}_p'$ and $\hat{x}\cdot\vec{h}_p'$ are given by (9) after replacing y by y'.

The plane $\eta = 0$ bisects the aperture, and it is convenient to write $\vec{e}_n''$ and $\hat{x}\cdot\vec{h}_n''$ in the form

$$\vec{e}_n'' = \hat{\eta}\sin\left(\frac{\pi x}{a}\right)f_n\left(\frac{2\eta}{d}\right), \qquad n = 0,1,2,\cdots$$

$$\hat{x}\cdot\vec{h}_n'' = \frac{j\omega\epsilon b}{2\pi}\left[\left(\frac{\lambda}{2a}\right)^2 - 1\right]\sin\left(\frac{\pi x}{a}\right)g_n\left(\frac{2\eta}{d}\right) \tag{11}$$

where $d = b - s$. The aperture functions $f_n(\xi)$ and $g_n(\xi)$ must be selected so that (2) is satisfied, but without loss of generality can be written in the form

$$f_n(\xi) = (-1)^n f_n(-\xi),$$

$$g_n(\xi) = (-1)^n g_n(-\xi). \tag{12}$$

It follows from (5) and (6) that $\underset{\sim}{A}$ has elements $A_{2n+1,2m+1} = 0$, enabling (5) to be separated into the two independent matrix equations $\underset{\sim}{A}^e\underline{b}^e = \underset{\sim}{Q}^e$ and $\underset{\sim}{A}^o\underline{b}^o = \underset{\sim}{Q}^o$, with $\underset{\sim}{Q}^o$ the null vector and $b_n^e = b_{2n}$, $b_n^o = b_{2n+1} = 0$. The aperture fields are therefore even about $\eta = 0$. The superscripts e and o are used throughout to denote variables associated with even and odd aperture functions, respectively.

The remaining matrix equation has elements

$$A_{n,m}^e = \frac{2d}{bD_{2n}}\sum_{p=0}^{\infty}\frac{\epsilon_p}{\gamma_P}\cos^2(\kappa_p)I_{2n,p}I_{2m,p},$$

$$n, m = 0,1,2\cdots$$

$$Q_n^e = \frac{2I_{2n,0}}{\gamma_0 D_{2n}} \tag{13}$$

where

$$\kappa_p = p\pi d/2b$$

and

$$I_{2n,p} = \int_0^1 f_{2n}(\xi)\cos(\kappa_p\xi)\,d\xi$$

$$D_{2n} = \int_0^1 f_{2n}(\xi)g_{2n}(\xi)\,d\xi$$

$$\epsilon_p = 1, \quad p = 0$$
$$= 2, \quad p > 0. \tag{14}$$

Orthogonality ensures that $I_{2n,0} = Q_n^e = 0, n > 0$, from which it can be shown that $l = \theta = 0$ and, therefore, the equivalent circuit of the E-plane displaced junction is a shunt susceptance in the junction plane.

$A_{0,0}^e$ is the only element of $\underset{\sim}{A}^e$ to contain a term in γ_0 and be complex, and the Appendix then shows that all b_n^e have the same argument. This enables the matrix equation to be separated into real and imaginary parts, and the problem reduces to solving

$$\underset{\sim}{W}^e\underset{\sim}{X}^e = \underset{\sim}{R}^e \tag{15}$$

where the real symmetric matrix $\underset{\sim}{W}^e$ and the real vector $\underset{\sim}{R}^e$ have elements

$$W_{n,m}^e = \sum_{p=0}^{\infty} \frac{\cos^2(\kappa_p)}{\gamma_p} H_{2n,p}H_{2m,p}, \qquad n, m = 0,1,2,\cdots$$

$$R_n^e = \frac{H_{0,0}}{[2\beta_0]^{1/2}}, \quad n = 0$$
$$= 0, \quad n > 0.$$

The $H_{2n,p}$ are obtained by dividing the $I_{2n,p}$ by a nonzero, but otherwise arbitrary, function of n, which will be denoted by $F^e(n)$.

The shunt susceptance and reflection coefficient are

$$\frac{B}{Y_0} = 2\alpha^e, \qquad \Gamma = \frac{-j\alpha^e}{1+j\alpha^e} \tag{17}$$

where the scalar α^e is calculated from

$$(\alpha^e)^{-1} = [\underset{\sim}{R}^e]^T\underset{\sim}{X} = R_0^e X_0^e. \tag{18}$$

A. Gegenbauer Polynomial Aperture Functions

To take into account the edge condition, the desired behavior of the transverse aperture field components is [5]

$$\vec{E}_T \propto \hat{y}r^{-1/3}, \qquad \hat{x}\cdot\vec{H}_T \propto r^{2/3}, \qquad \text{as } r \to 0 \tag{19}$$

where r in Fig. 2 is the distance from an edge, measured in the aperture plane. Orthogonal aperture functions, which each behave correctly near the edges, can be written in terms of the Gegenbauer polynomials $C_n^{\nu}(\xi)$ as

$$f_n(\xi) = (1-\xi^2)^{-1/3}C_n^{5/6}(\xi)$$
$$g_n(\xi) = (1-\xi^2)^{2/3}C_n^{5/6}(\xi). \tag{20}$$

These give rise to integrals for the $H_{2n,p}$ which can be evaluated as an infinite summation of hypergeometric functions, but a simpler result is obtained if the aperture functions are chosen to be the orthogonal set

$$f_n(\xi) = (1-\xi^2)^{-1/3}C_n^{1/6}(\xi)$$
$$g_n(\xi) = C_n^{1/6}(\xi) \tag{21}$$

which correctly describes the behavior of $\vec{E}_T$ at the edges, and approximates the behavior of $\hat{x}\cdot\vec{H}_T$ at the edges when several functions are summed. The integrals for the $H_{2n,p}$ can be evaluated using [10]

$$\int_{-1}^{1}(1-\xi^2)^{\nu-1/2}C_n^{\nu}(\xi)\exp(j\kappa\xi)\,d\xi = \frac{j^n 2\pi\Gamma(n+2\nu)J_{n+\nu}(\kappa)}{\Gamma(n+1)\Gamma(\nu)(2\kappa)^{\nu}}, \qquad \mathrm{Re}(\nu) > -1/2 \tag{22}$$

and $F^e(n)$ chosen such that

$$H_{2n,p} = \frac{J_{2n+1/6}(\kappa_p)}{(\kappa_p)^{1/6}}, \qquad p > 0$$

$$H_{0,0} = \frac{(3\pi)^{1/2}2^{7/6}}{[\Gamma(1/3)]^2} \tag{23}$$

where $J_{\nu}(z)$ is the Bessel function of the first kind, and $\Gamma(z)$ is the Gamma function.

In order to invert $\mathbf{W}^e$, the aperture functions considered must be restricted to a finite number N, but in principle it is not necessary to limit the number of waveguide modes considered. However, for speed of computation, we use (23) to consider P waveguide modes exactly, and the asymptotic expression

$$J_{\nu}(z) \to \left(\frac{2}{\pi z}\right)^{1/2}\cos\left(z - \frac{\nu\pi}{2} - \frac{\pi}{4}\right), \qquad z \to \infty \tag{24}$$

to obtain a residual R which approximates the contribution to $W_{n,m}^e$ from higher waveguide modes. Thus

$$W_{n,m}^e \simeq \sum_{p=1}^{P-1}\frac{\cos^2(\kappa_p)}{\gamma_p(\kappa_p)^{1/3}}J_{2n+1/6}(\kappa_p)J_{2m+1/6}(\kappa_p) + (-1)^{n+m}R$$

$$R = \frac{1}{2\pi}\sum_{p=P}^{\infty}\frac{[\cos(2\kappa_p - \pi/3) - 1/2]^2}{\gamma_p(\kappa_p)^{4/3}}. \tag{25}$$

B. Trigonometric Aperture Functions

Aperture functions which have the same form as waveguide modes are

$$f_{2n}(\xi) = g_{2n}(\xi) = \cos(n\pi\xi) \tag{26}$$

and by choosing $F^e(n) = (-1)^n$

$$H_{2n,p} = \frac{\kappa_p\sin(\kappa_p)}{(\kappa_p)^2 - (n\pi)^2}, \qquad \kappa_p \neq n\pi \tag{27}$$

and $H_{0,0} = 1$. As the denominator δ in (27) tends to zero

$$H_{2n,p} \to \frac{(-1)^n}{2}\left(1 + \frac{\delta}{2n\pi}\right), \qquad \delta \to 0. \tag{28}$$

IV. *H*-Plane Displacement

The displaced junction in Fig. 3 shows waveguide 2 in the x', y, z cartesian coordinate system displaced by an amount $x = s$ with respect to waveguide 1 in the x, y, z cartesian coordinate system. With a TE_{10}-mode signal of free-space wavelength λ incident from waveguide 1, the TE_{p0} modes set up by the discontinuity will have components

$$\vec{e}_p = \hat{y}\sin\left(\frac{p\pi x}{a}\right), \qquad p = 1,2,3,\cdots$$

$$\vec{h}_p = \hat{x}j\left(\frac{\epsilon}{\mu}\right)^{1/2}\frac{\lambda}{a}\gamma_p\sin\left(\frac{p\pi x}{a}\right) \tag{29}$$

where $\vec{e}_{1,0} \equiv \vec{e}_1$, and γ_p is related to the propagation constant γ_p' of mode p, which is evanescent for $p \geq 2$, by

$$\gamma_p = \frac{a}{2\pi}\gamma_p' = \left[\left(\frac{p}{2}\right)^2 - \left(\frac{a}{\lambda}\right)^2\right]^{1/2}, \qquad p = 2,3,4,\cdots$$

$$\gamma_1 = j\beta_1 = j\left[\left(\frac{a}{\lambda}\right)^2 - \frac{1}{4}\right]^{1/2}. \tag{30}$$

Expressions for $\vec{e}_p'$ and $\vec{h}_p'$ are given by (29) after replacing x by x'.

The plane $\eta = 0$ bisects the aperture, and we write

$$\vec{e}_n'' = \hat{y}f_n\left(\frac{2\eta}{d}\right), \qquad n = 0,1,2,\cdots$$

$$\vec{h}_n'' = \hat{\eta}j\left(\frac{\epsilon}{\mu}\right)^{1/2}\frac{\lambda}{a}g_n\left(\frac{2\eta}{d}\right) \tag{31}$$

where the aperture functions are selected so that (2) and (12) are satisfied.

The analysis for the *H*-plane displacement case is similar to that for *E*-plane displacement, with elements $A_{2n+1,2m+1} = 0$, enabling (5) to be separated into two independent matrix equations which can each be put into the form discussed in the Appendix. The problem reduces to solving

$$\underset{\sim}{W}^e\underset{\sim}{X}^e = \underset{\sim}{R}^e, \qquad \underset{\sim}{W}^o\underset{\sim}{X}^o = \underset{\sim}{R}^o \tag{32}$$

where the real, symmetric matrices $\underset{\sim}{W}^e, \underset{\sim}{W}^o$ and the real vectors $\underset{\sim}{R}^e$, $\underset{\sim}{R}^o$ have elements

$$W^e_{n,m} = \sum_{p=2}^{\infty}\gamma_p\sin^2(\kappa_p)H_{2n,p}H_{2m,p}, \qquad n,m = 0,1,2\cdots$$

$$W^o_{n,m} = \sum_{p=2}^{\infty}\gamma_p\cos^2(\kappa_p)H_{2n+1,p}H_{2m+1,p}, \qquad n,m = 0,1,2\cdots$$

$$R^e_n = \beta_1^{1/2}\sin(\kappa_1)H_{2n,1}$$

$$R^o_n = \beta_1^{1/2}\cos(\kappa_1)H_{2n+1,1} \tag{33}$$

with

$$\kappa_p = p\pi d/2a$$

and

$$H_{2n,p} = \int_0^1 f_{2n}(\xi)\cos(\kappa_p\xi)\,d\xi/F^e(n)$$

$$H_{2n+1,p} = \int_0^1 f_{2n+1}(\xi)\sin(\kappa_p\xi)\,d\xi/F^o(n). \tag{34}$$

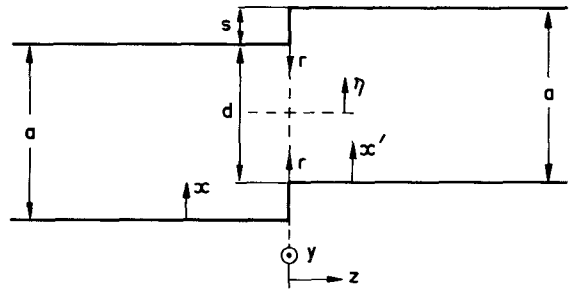

Fig. 3 Geometry of an *H*-plane displaced junction.

$F^e(n)$ and $F^o(n)$ are nonzero, but otherwise arbitrary, functions of n.

The equivalent circuit elements and the reflection coefficient are

$$\frac{B}{Y_0} = \frac{2(1+\alpha^e\alpha^o)}{\alpha^e - \alpha^o}$$

$$\theta = \pi - 2\tan^{-1}(\alpha^o)$$

$$\Gamma = (1 - j\alpha^e)^{-1} + (1 - j\alpha^o)^{-1} - 1 \tag{35}$$

where the scalars α^e and α^o are calculated from

$$(\alpha^e)^{-1} = \left[\underset{\sim}{R}^e\right]^T\underset{\sim}{X}^e$$

$$(\alpha^o)^{-1} = \left[\underset{\sim}{R}^o\right]^T\underset{\sim}{X}^o. \tag{36}$$

A. Gegenbauer Polynomial Aperture Functions

To take into account the edge condition, the desired behavior of the transverse aperture fields is [5]

$$\vec{E}_T \propto \hat{y}r^{2/3}, \qquad \vec{H}_T \propto \hat{x}r^{-1/3}, \qquad \text{as } r \to 0 \tag{37}$$

where r is shown in Fig. 3. Orthogonal aperture functions which each behave correctly near the edges are given by (20), with the expressions for $f_n(\xi)$ and $g_n(\xi)$ interchanged. Interchanging the expressions for $f_n(\xi)$ and $g_n(\xi)$ in (21) enables (22) to be used with an alternate formulation to (5) in terms of the unknown coefficients $\{c_n\}$, and ensures that $\vec{H}_T$ behaves correctly at the edges, and approximates the behavior of $\vec{E}_T$ at the edges when several functions are summed. However, numerical comparisons showed more rapid convergence using (5) and (22) with

$$f_n(\xi) = (1-\xi^2)^{2/3}C_n^{7/6}(\xi)$$

$$g_n(\xi) = C_n^{7/6}(\xi) \tag{38}$$

which correctly describes the behavior of $\vec{E}_T$ at the edges, and approximates the behavior of $\vec{H}_T$ when several functions are summed. Obvious choices of $F^e(n)$ and $F^o(n)$ result in

$$H_{n,p} = \frac{J_{n+7/6}(\kappa_p)}{(\kappa_p)^{7/6}}. \tag{39}$$

As before, we consider P waveguide modes exactly, and use (24) to obtain residuals $R^{\pm}$ which approximate the

contribution from higher waveguide modes. Thus

$$W^e_{n,m} \simeq \sum_{p=2}^{P} \frac{\gamma_p \sin^2(\kappa_p)}{(\kappa_p)^{7/3}} J_{2n+7/6}(\kappa_p) J_{2m+7/6}(\kappa_p) + (-1)^{n+m} R^+$$

$$W^o_{n,m} \simeq \sum_{p=2}^{P} \frac{\gamma_p \cos^2(\kappa_p)}{(\kappa_p)^{7/3}} J_{2n+13/6}(\kappa_p) J_{2m+13/6}(\kappa_p) + (-1)^{n+m} R^-$$

$$R^{\pm} = \frac{1}{2\pi} \sum_{p=P+1}^{\infty} \frac{\gamma_p \left[\sin(2\kappa_p + \pi/6) \mp 1/2\right]^2}{(\kappa_p)^{10/3}}. \quad (40)$$

B. Trigonometric Aperture Functions

Aperture functions having the form of waveguide modes are

$$f_n(\xi) = g_n(\xi) = \sin\left[(n+1)(\xi+1)\frac{\pi}{2}\right] \quad (41)$$

which lead to

$$H_{2n,p} = \frac{\cos(\kappa_p)}{\left[(2n+1)\frac{\pi}{2}\right]^2 - (\kappa_p)^2}$$

$$H_{2n+1,p} = \frac{\sin(\kappa_p)}{[(n+1)\pi]^2 - (\kappa_p)^2}. \quad (42)$$

As the denominators δ in (42) tend to zero

$$H_{2n,p} \to \frac{(-1)^n}{(2n+1)\pi}\left[1 + \frac{\delta}{(2n+1)\pi}\right], \quad \delta \to 0$$

$$H_{2n+1,p} \to \frac{(-1)^n}{2(n+1)\pi}\left[1 + \frac{\delta}{2(n+1)\pi}\right], \quad \delta \to 0. \quad (43)$$

V. Results

If N aperture functions are considered in the preceding matrix formulations, the orders of $\mathbf{W}^e$ and $\mathbf{W}^o$ are $I\{(N+1)/2\}$ and $I\{N/2\}$, respectively, where $I\{\ \}$ signifies "the integer part of."

It has been found [6], [11] that, for the trigonometric aperture function formulations (TF), convergent solutions are most readily achieved if the number of aperture functions has a value close to $N = I\{PA_a/A_1\}$, and this relationship is used in all our TF computations.

The value of N required for convergence is much less using the Gegenbauer polynomial formulations (GF) than TF with the same value of P. For example, an E-plane displacement of $s/b = 0.1$ with $b/\lambda_g = 0.3$ has an equivalent circuit normalized shunt susceptance of $B/Y_0 = 0.058041$. With $P = 100$, the TF ($\underset{\sim}{W}^e$ of order 45) gave the answer correct to five decimal places, but the same convergence was achieved with the GF when $\underset{\sim}{W}^e$ was of order 3.

With $P = 100$, values of $|\Gamma|$ from the TF were convergent to at least five decimal places for $0.05 \leqslant A_a/A_1 \leqslant 0.99$.

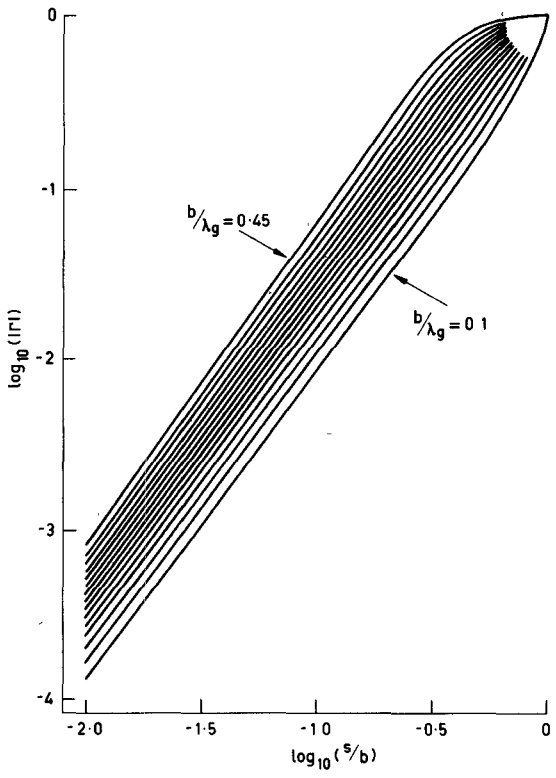

Fig. 4. Reflection coefficient magnitude for an E-plane displaced junction, with $b/\lambda_g = .1\ (.025)\ .45$.

Equal or better convergence was found using the GF with $N = 12$ for $A_a/A_1 \geqslant 0.9$, $N = 8$ for $0.5 \leqslant A_a/A_1 < 0.9$, and $N = 4$ for $A_a/A_1 < 0.5$.

The effect of neglecting the residual term in the GF matrix elements was examined, and, irrespective of the number of aperture functions considered, the accuracy of the results did not equal that of the TF using the same value of P. This is attributed to terms in the matrix elements decreasing as p^3 for the TF, but only as $p^{7/3}$ for the GF, making the neglect of higher terms more significant.

The GF requires the evaluation of a large number of Bessel functions, and, although these can be computed rapidly using backward recurrence, the computation of the trigonometric functions required for the TF is somewhat faster. However, once the Bessel functions (or trigonometric functions) have been evaluated for a given displacement, the smaller matrix size needed with the GF renders that method increasingly superior as the number of frequencies of interest increases. When the displacement is large (aperture small), the reduced matrix size required by the TF reduces the GF superiority.

The computations were verified to within the experimental accuracy of a six-port reflectometer measurement [12]. Reflection coefficients were measured in WR284 waveguide, for both E-plane and H-plane displacements.

Figs. 4 and 5 show the variation of $|\Gamma|$ and B/Y_0 with E-plane displacement for various values of b/λ_g. At a fixed frequency, $|\Gamma|$ increases monotonically with displacement, and for a given displacement it increases monotoni-

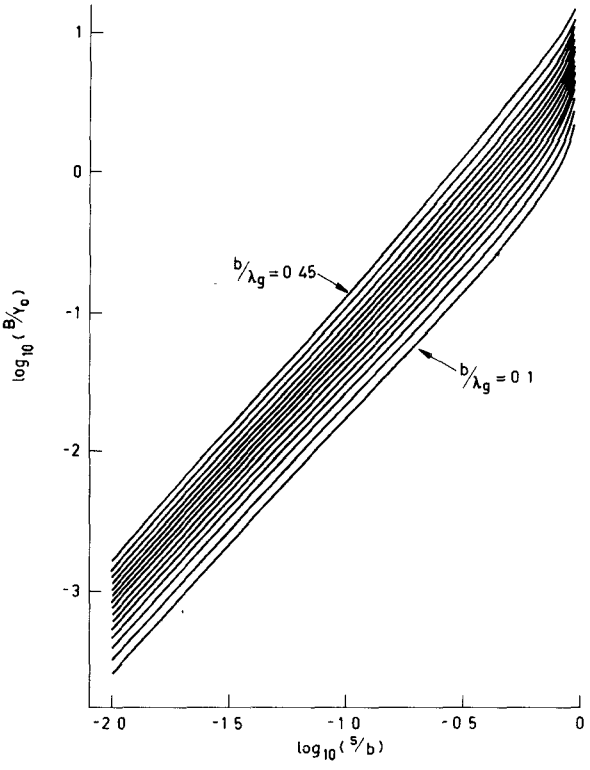

Fig 5. Equivalent circuit normalized shunt susceptance for an E-plane displaced junction, with $b/\lambda_g = .1\ (.025)\ .45$.

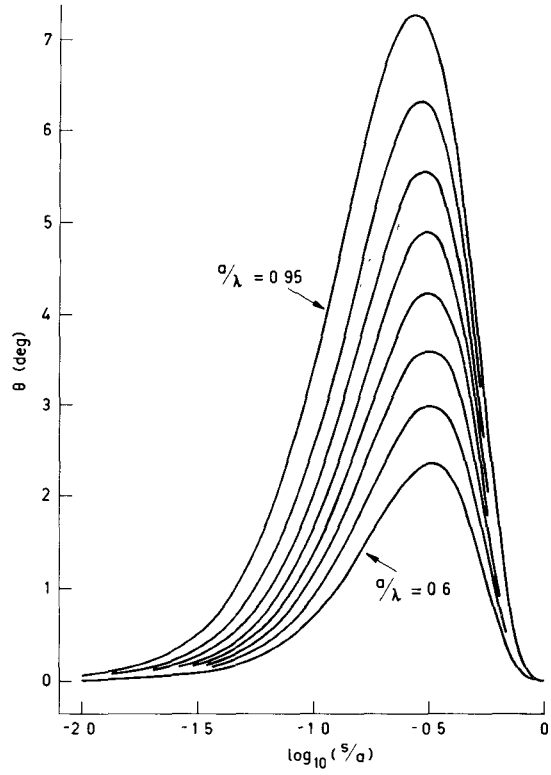

Fig. 6. Extra electrical-line length introduced by an H-plane displaced junction, with $a/\lambda = .6\ (.05)\ .95$.

TABLE I
POLYNOMIAL COEFFICIENTS FOR APPROXIMATION TO $|\Gamma|$ IN (44)

n	E-Plane Displacement u_n	E-Plane Displacement v_n	H-Plane Displacement u_n	H-Plane Displacement v_n
0	1.833	0.293	1.750	0.635
1	0.276	2.133	-0.332	-1.562
2	0.73	0.78	-2.71	0.44
3	0	19.69	-3.57	-7.63

cally with frequency. For $0.1 \leqslant b/\lambda_g \leqslant 0.45$, $|\Gamma|$ can be approximated by

$$\log_{10}(|\Gamma|) \simeq \sum_{n=0}^{3} u_n(\xi-\alpha)^n \log_{10}(\tau) + \sum_{n=0}^{3} v_n(\xi-\alpha)^n \tag{44}$$

with $\xi = b/\lambda_g$, $\alpha = 0.3$, $\tau = s/b$, and the coefficients u_n, v_n given in Table I. This gives $|\Gamma|$ with an error of less than $1\frac{1}{2}$ percent for $0.025 \leqslant s/b \leqslant 0.25$, and with an absolute error of less than 0.0001 for $s/b < 0.025$. B/Y_0 and $\arg(\Gamma)$ are calculable from (8), taking $\operatorname{sgn}(B/Y_0) = 1$ and $\theta = 0$.

The effective extra electrical length θ introduced by H-plane displacement of the junction is shown in Fig. 6, and never exceeds $7\frac{1}{2}$ degrees. Fig. 7 shows the variation of $|\Gamma|$ with H-plane displacement for various values of a/λ. At a fixed frequency, $|\Gamma|$ increases monotonically with displacement, but it decreases monotonically with frequency only for large displacements. The expression in (44) can

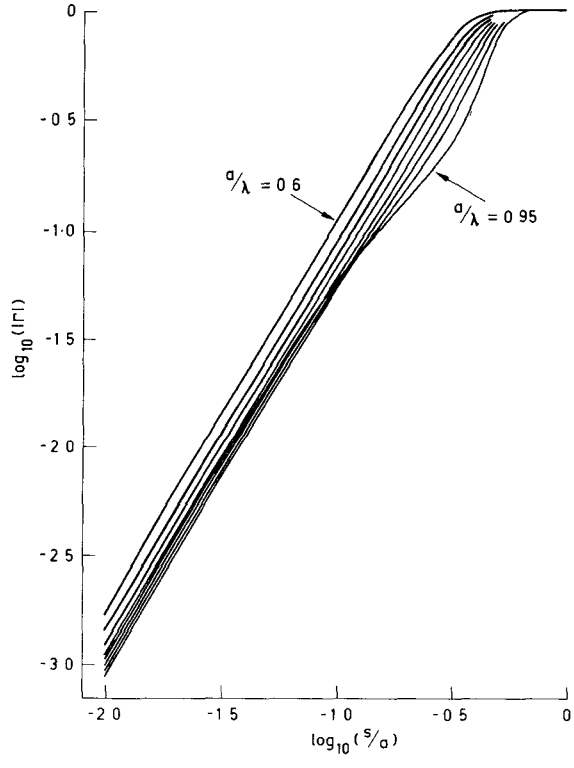

Fig. 7. Reflection coefficient magnitude for an H-plane displaced junction, with $a/\lambda = .6\ (.05)\ .95$.

be used with the coefficients in Table I and $\xi = a/\lambda$, $\alpha = 0.7$, $\tau = s/a$, to approximate $|\Gamma|$ with an error of less than 4 percent for $0.6 \leqslant a/\lambda \leqslant 0.9$, $0.05 \leqslant s/a \leqslant 0.25$. For $0.6 \leqslant a/\lambda \leqslant 0.95$, $s/a < 0.05$, the approximation gives $|\Gamma|$ with an absolute error of less than 0.0015, and for $0.9 < a/\lambda \leqslant 0.95$ the absolute error is less than 0.008 for $s/a \leqslant 0.2$, and less than 0.015 for $s/a \leqslant 0.25$. B/Y_0 and $\arg(\Gamma)$ are calculable from (8) after taking $\operatorname{sgn}(B/Y_0) = -1$, and using the curves in Fig. 6 to estimate θ.

VI. A Displaced Junction as a Reference Reflection

Reduced-height waveguides are well established as a means of providing reference reflections in a rectangular waveguide system. To a first order of accuracy, the reflection coefficient is simply related to the ratio of waveguide heights, and is frequency independent. For more accurate work, the frequency dependence of the reflection can be estimated using an approximate formula which takes into account the capacitance associated with the waveguide step [1]. The effect of the loss associated with the flange junction should also be considered, as it affects the calculated value of the reflection coefficient directly [13]. A set of reduced-height waveguides providing a range of (fixed) reference reflections can be costly to manufacture.

The displaced waveguide junction is an alternative means of providing a reference reflection, with the major advantage that a single junction, made by attaching oversized flanges to two lengths of precision waveguide, can be appropriately displaced to produce any value of $|\Gamma|, 0 \leqslant |\Gamma| \leqslant 1$. The reflection coefficient for a given displacement is calculated readily using the preceding analysis, and for small displacements, the effect of flange loss is minimized, as it is in quadrature with the calculated reflection. An E-plane displaced junction has the particular advantages of a simple equivalent circuit, namely, a shunt susceptance in the plane of the junction, and the availability of a simple approximate formula (44) which is sufficiently accurate, for displacements of up to 25 percent, that it can be used in all but the most exacting circumstances.

A disadvantage of this use of a displaced junction is that $|\Gamma|$ is approximately twice as sensitive to mechanical measurement error than when a reduced-height waveguide is used. The displaced junction is also more frequency sensitive than a reduced-height guide, but this is only a disadvantage if wide-band measurements are contemplated.

VII. Conclusions

Matrix equations have been developed to describe the effect of a displaced junction in rectangular waveguide, and to determine the equivalent circuit parameters. Weighted Gegenbauer polynomials were used to improve the representation of the aperture fields near the edges and, as a consequence, the matrix solutions converged rapidly. Approximate formulas derived from the results apply for displacements up to 25 percent of the waveguide dimensions.

The effects of E-plane or H-plane displacement are quite different in character. Although the effect of H-plane displacement can be represented by a shunt susceptance and an increase in the electrical length of the waveguide, the effect of E-plane displacement can be represented solely by a shunt susceptance in the displacement plane. The advantages and disadvantages of using an E-plane displaced junction as an adjustable reference have been discussed.

Appendix

Inversion of a Matrix with Complex Elements only in the First Row. Consider a matrix $\underset{\sim}{A}$ of order $N+1$ and its inverse $\underset{\sim}{A}^{-1}$ where

$$\underset{\sim}{A} = \left(\begin{array}{c|c} \underset{\sim}{D} & \underset{\sim}{F} \\ \hline \underset{\sim}{E} & \underset{\sim}{G} \end{array}\right), \qquad \underset{\sim}{A}^{-1} = \left(\begin{array}{c|c} \underset{\sim}{U} & \underset{\sim}{W} \\ \hline \underset{\sim}{V} & \underset{\sim}{X} \end{array}\right)$$

$\underset{\sim}{D}$ and $\underset{\sim}{U}$ contain single elements, $\underset{\sim}{F}$ and $\underset{\sim}{W}$ are row vectors of length N, $\underset{\sim}{E}$ and $\underset{\sim}{V}$ are column vectors of length N, and $\underset{\sim}{G}$ and $\underset{\sim}{X}$ are square matrices of order N. Since $\underset{\sim}{A}\underset{\sim}{A}^{-1} = \underset{\sim}{I}$, it follows that

$$\underset{\sim}{V} = -\underset{\sim}{G}^{-1}\underset{\sim}{E}\underset{\sim}{U}.$$

Hence, if $\underset{\sim}{E}$ and $\underset{\sim}{G}$ are real, all elements in the first column of $\underset{\sim}{A}^{-1}$ have the same argument. In particular, if

$$\underset{\sim}{A}\underset{\sim}{b} = \underset{\sim}{Q}$$

where $\underset{\sim}{Q}$ is a column vector with all elements zero except the first, the elements of the vector $\underset{\sim}{b}$ will have the same argument.

Acknowledgment

Many helpful discussions with P. I. Somlo and I. G. Morgan are gratefully acknowledged, as is the assistance of G. R. Allen in making the adjustable displaced junction and P. I. Somlo in performing the six-port measurements.

References

[1] N. Marcuwitz, *Waveguide Handbook*. New York: McGraw-Hill, 1951.

[2] U. von Kienlin and A. Kurzl, "Reflexionen an hohlleiterflanschverbindungen," *Nachrichtentech. Z. (NTZ)*, pp. 561–564, 1958.

[3] P. J. B. Clarricoats and K. R. Slinn, "Numerical method for the solution of waveguide-discontinuity problems," *Electron. Lett.*, vol. 2, pp. 226–228, 1966.

[4] A. Wexler, "Solution of waveguide discontinuities by modal analysis," *IEEE Trans. Microwave Theory Tech.*, vol. MTT-15, pp. 508–517, 1967

[5] R. Mittra and S. W. Lee, *Analytical Techniques in the Theory of Guided Waves*. New York: Macmillan, 1971.

[6] P. H. Masterman and P. J. B. Clarricoats, "Computer field-matching solution of waveguide transverse discontinuities," *Proc. Inst. Elec. Eng.*, vol. 118, pp. 51–63, 1971.

[7] R. Safavi-Naini and R. H. MacPhie, "Scattering at rectangular-to-rectangular waveguide junctions," *IEEE Trans. Microwave Theory Tech.*, vol. MTT-30, pp. 2060–2063, 1982.

[8] C. Vassallo, "On a direct use of edge condition in modal analysis," *IEEE Trans. Microwave Theory Tech.*, vol. MTT-24, pp. 208–212, 1976.

[9] V. P. Lyapin, V. S. Mikhalevsky and G. P. Sinyavsky, "Taking into account the edge condition in the problem of diffraction waves on step discontinuity in plate waveguide," *IEEE Trans. Microwave Theory Tech.*, vol. MTT-30, pp. 1107–1109, 1982.

[10] I. S. Gradshteyn and I. W. Ryzhik, *Table of Integrals, Series, and Products*. New York: Academic Press, section 7.32, 1965.
[11] S. W. Lee, W. R. Jones, and J. J. Campbell, "Convergence of numerical solutions of iris-type discontinuity problems," *IEEE Trans. Microwave Theory Tech.*, vol. MTT-19, pp. 528–536, 1971.
[12] P. I. Somlo and J. D. Hunter, "A six-port reflectometer and its complete characterization by convenient calibration procedures," *IEEE Trans. Microwave Theory Tech.*, vol. MTT-30, pp. 186–192, 1982.
[13] P. I. Somlo, "The effect of flange loss on the reflection coefficient of reduced-height waveguide reflection standards," *IEEE Trans. Microwave Theory Tech.*, vol. MTT-27, pp. 795–797, 1979.

John D. Hunter (S'68–M'79–SM'83) received the B.E. (Hons.) and Ph.D. degrees in electrical engineering from the University of Canterbury, New Zealand, in 1967 and 1970, respectively.

He taught at the University of Canterbury from 1970–71, and then worked on electromagnetic scattering problems as a Post-Doctoral Fellow at the University of Manitoba in 1971–73. Since joining the CSIRO Division of Applied Physics in Sydney in 1973, he has been developing measurement systems at radio and microwave frequencies, with a particular interest in antenna measurements.

Theoretical Analysis of Intermodulation Distortion of Reflection-Type IMPATT Amplifiers

MOUSTAFA EL-GABALY, SENIOR MEMBER, IEEE, AND M. EZZAT EL-SHANDWILY, MEMBER, IEEE

Abstract—**The basic equations for a reflection-type IMPATT amplifier are used to derive expressions for the output when the amplifier is driven by a multifrequency input signal. The third-order intermodulation distortion is expressed and graphically presented for various diode, circuit, and signal parameters. The results provide a guideline for designing amplifiers with minimum intermodulation distortion or prescribed distortion level.**

I. INTRODUCTION

IMPATT amplifiers are used in microwave communication systems and are expected to find wide applications in millimeter-wave satellite communications. Due to the inherent nonlinearity of the device, when more than one signal is applied to the amplifier input, intermodulation components will result. Some of these components are usually within the bandwidth of the amplifier circuit and appear in the output as intermodulation distortion.

Several investigators used the Volterra series technique to analyze the small-signal nonlinearity of microwave devices [1]–[16]. The main idea in all these analyses is to represent the device by an equivalent circuit with nonlinear elements. The nonlinearity of the elements (such as conductance, capacitance, and transconductance) is represented by a power series of the applied RF voltage. Measurement of these parameters as functions of the RF voltage for the particular device used is then carried out. In IMPATT devices, the measured negative conductance and device susceptance as functions of RF voltage amplitude are usually used to determine the power-series coefficients through curve-fitting techniques. Investigations of this type suffer from two limitations. First, the process of measurement and curve fitting has to be carried out for each device to find the coefficients of the power series expansion for the device elements. Second, the effect of the physical parameters of the device (such as doping profile, dimensions, etc.) is not explicitly shown.

Recently, Best *et al.* [17] used a different approach to obtain the nonlinear response of a reflection IMPATT amplifier to the amplitude of the combined input signals in the time domain. They also used the measured nonlinear diode conductance for numerical calculations.

This paper investigates the intermodulation distortion of an IMPATT amplifier with a Read doping profile. The basic equations for the operation of the IMPATT device driven by a multifrequency RF voltage are used to obtain the output. The analysis is general, and it suffices to know the device parameters: phase delay $\omega\tau$, drift capacitance, avalanche frequency ω_a (or, equivalently, the small-signal admittance and ω_a), and the external circuit parameters to determine the intermodulation distortion. This avoids the extensive large-signal admittance measurements and the

Manuscript received June 15, 1983; revised October 31, 1983. This work was supported by the Kuwait University Research Council under Grant EE008.

M. El-Gabaly is with the Department of Electrical and Computer Engineering, University of Michigan, Ann Arbor, MI 48109, on leave from the Department of Electrical Engineering, Kuwait University, Kuwait.

M. E. El-Shandwily is with the Department of Electrical Engineering, University of Kuwait, Kuwait.

0018-9480/84/0400-0394$01.00 ©1984 IEEE